JOURNAL OF APPLIED PHYSICS 115, 133904 (2014)

Structural and magnetic characterization of as-prepared and annealed FeCoCu nanowire arrays in ordered anodic aluminum oxide templates

B. Rodríguez-González,[1,2,a)] C. Bran,[3] T. Warnatz,[3] J. Rivas,[2] and M. Vazquez[3]
[1]CACTI, University of Vigo, E-36310 Vigo, Spain
[2]International Iberian Nanotechnology Laboratory, INL. Av. Mestre J. Veiga, 4715-330 Braga, Portugal
[3]Institute of Materials Science of Madrid, CSIC, 28049 Madrid, Spain

(Received 12 January 2014; accepted 21 March 2014; published online 2 April 2014)

Herein, we report on the preparation, structure, and magnetic characterization of FeCoCu nanowire arrays grown by DC electrodeposition inside self-assembled ordered nanopores of anodic aluminum oxide templates. A systematic study of their structure has been performed both in as-prepared samples and after annealing in the temperature range up to 800 °C, although particular attention has been paid to annealing at 700 °C after which maximum magnetic hardening is achieved. The obtained nanowires have a diameter of 40 nm and their $Fe_{0.28}Co_{0.67}Cu_{0.05}$ composition was confirmed by energy dispersive X-ray spectroscopy (EDS). Focused ion-beam lamellas of two samples (as-prepared and annealed at 700 °C) were prepared for their imaging in the high-resolution transmission electron microscopy (HRTEM) perpendicularly to the electron beam, where the obtained EDS compositional mappings show a homogeneous distribution of the elements. X-ray diffraction analysis, and selected area electron diffraction (SAED) patterns confirm that nanowires exhibit a *bcc* cubic structure (space group Im-3m). In addition, bright-dark field images show that the nanowires have a polycrystalline structure that remains essentially the same after annealing, but some modifications were observed: (i) an overall increase and sharpening of recrystallized grains, and (ii) an apparent shrinkage of the nanowires diameter. Obtained SAED patterns also show strong textured components with determined $\langle 111 \rangle$ and $\langle 112 \rangle$ crystalline directions parallel to the wires growth direction. The presence of both directions was also confirmed in the HRTEM images doing Fourier transform analyses. Magnetic measurements show strong magnetic anisotropy with magnetization easy axis parallel to the nanowires in as-prepared and annealed samples. The magnetic properties are tuned by suitable thermal treatments so that, maximum enhanced coercivity (~2.7 kOe) and normalized remanence (~0.91 Ms) values are achieved after annealing at temperature of 700 °C. The contribution of the changes in the crystalline structure, induced by the heat treatment, to the magnetic hardening of the FeCoCu nanowires is discussed. [http://dx.doi.org/10.1063/1.4870289]

I. INTRODUCTION

Porous membranes are currently considered as convenient and useful templates for the electrochemical growth of different kinds of nanomaterials, particularly long-range ordered nanowire arrays.[1,2] Among others, magnetic nanowire arrays are being increasingly investigated in various applications as potential advanced media of magnetic storage, in microwave technologies, or for magnetic and biomagnetic functionalization.[3,4] In addition, they are considered as nearly ideal systems for micromagnetic studies in cylindrical magnetic systems.[5] In that regard, their magnetization reversal is typically determined by the energy balance between shape and magnetocrystalline anisotropies, as well as by their magnetostatic interactions. While nanowires out of Fe and Ni and their alloys (i.e., Permalloy) exhibit reduced crystalline anisotropy, which is usually overcome by their geometrically intrinsic shape magnetic anisotropy, Co based nanowires show enhanced magnetocrystalline anisotropy that can determine the effective magnetization easy axis.[6–8] Crystalline structure can be tuned conveniently by appropriate choosing of synthesis parameters, which consequently will play an important role to determine the magnetic properties of nanowire arrays.[9–11]

The electrochemical route for growing nanowires within those templates comprises the obtaining of the template with self-assembled nanopores and their subsequent filling with the metallic material. Several methods have been established depending on the composition of the template and on the wires deposition technique.[12] The composition of the templates is generally limited to polymer films and anodized aluminum membranes. Pores in polymer films are mostly randomly distributed because they are obtained by etching films previously exposed to radiation, and their diameter is also variable.[13,14] Anodized aluminum oxide (AAO) membranes are prepared by controlled anodization of aluminum foils in acid medium.[15] Usually they are made of cylindrical-shaped pores of constant diameter, surrounded by aluminum oxide, and packed in hexagonal regular arrays. The diameter and length of pores, as well as the interpore distance, can be easily controlled by varying the anodization parameters that make the AAO membranes an optimum choice for the growing of metallic nanowires arrays with tailored magnetic properties.

[a)]Author to whom correspondence should be addressed. Electronic mail: jbenito@uvigo.es

Several experimental techniques have been reported to grow the nanowires inside the pores of a template as electrophoretic deposition, vapor injection, liquid injection, chemical or electrochemical deposition.[16,17] In the case of metallic nanowires, the most common fabrication method is the electrodeposition in liquid solution.[18,19] In addition to its cost-effectiveness, electrodeposition is one of the few methods that can overcome the geometrical restrictions of inserting metals into very long nanometric pores, and provides an efficient way to produce magnetic nanowire arrays with high aspect ratio. As it has been demonstrated, the metal alloy composition and its crystallographic structure can be tuned by controlling the deposition conditions (applied potential, pH, bath temperature, and concentration), which finally determine the magnetic properties of resulting nanowires.[10,20–26] While most reports are addressed to magnetic properties of metallic nanowires, relatively less attention has been paid to full structure characterization, and especially after submitting the samples to thermal treatments.[27,28]

Particular interest of FeCo nanowires lies in their high saturation magnetization and Curie temperature (which enables working at more elevated temperature). Despite the number of works devoted to the fabrication of FeCo nanowire arrays, only few studies are devoted to unveil the structure/morphology of the nanowires-AAO composite and the crystalline growth direction inside the template. The general approach to achieve such information is the wet etching of the AAO template and the deposition of the wires over a new substrate to obtain the X-ray diffraction (XRD) pattern. However, this method implies the loss of the initial crystalline orientation relationship in the array, leading in some cases to incomplete sample characterization. The loss of the initial structure of the sample can be partially overcome using the focused ion beam (FIB) sample preparation, followed by a deep transmission electron microscopic (TEM) study of the sample. FIB has been widely used in TEM sample preparation of different types of magnetic samples such as films, hybrid materials, particles, and wires.[29]

In this work, we have obtained FeCoCu nanowire arrays electroplated into AAO templates, where the presence of a limited amount of Cu has been claimed to be effective to promote a magnetic hardening of FeCo nanowires.[28] The main objective of this work has been the systematic characterization of the nanowires structure particularly focusing on the effect of the thermal treatment. The study is complemented with the magnetic characterization at room temperature after such treatments.

We should underline that present studies were performed on nanowires while embedded into the membranes. Cross-section FIB sample preparation seems to be convenient in the present case since it preserves the structure and the arrangement of the wires inside the AAO template. In particular, we have prepared two lamellas, one obtained from the as-prepared sample and other from the sample annealed at 700 °C. Simultaneous to the lamella fabrication in the FIB, SEM images were obtained, as well as relevant microanalysis to confirm the nanowires composition. Moreover, cross-section lamellas were prepared to allow for the TEM imaging of the wires with their longitudinal axis perpendicular to the electron beam. This geometry enabled the simultaneous use of different electron microscopy characterization techniques such as high-resolution transmission electron microscopy (HRTEM), selected area electron diffraction (SAED), scanning-transmission electron microscopy (STEM), and energy dispersive X-ray spectroscopy (EDS). Consequently, data were obtained about the composition and crystalline structure of wires, their geometry features as diameter and length, and their homogeneity.

II. EXPERIMENTAL PROCEDURE

Magnetic nanowires were prepared by electroplating filling of self-assembled pores in AAO templates. The ordered AAO membranes were synthesized by two-step anodization process on 99.999% Al foils in oxalic acid 0.3M electrolyte by applying a constant voltage of 40 V and keeping the temperature between 4 and 6 °C. The first anodization was performed for 24 h and the second one was performed for 20 h to assure a thickness of nanoporous alumina template of about 40 μm. Afterwards, the Al was chemically etched from the bottom side (upper side in Figures 1(b)–1(d)) followed by the removal of the barrier layer and enlargement of the pores using H_3PO_4 (5%wt.). An Au metallic nanolayer was sputtered to serve later as an electrode for final electroplating of nanowires.

FeCoCu alloy nanowires were deposited into the AAO membranes at room-temperature by DC electrodeposition in a three electrode electrochemical cell equipped with an Ag/AgCl reference electrode, an insoluble platinum mesh counter electrode, and an Au coated membrane acting as a working electrode. The wires were grown using a single sulfate-based electrolyte containing $CoSO_4 \cdot 7H_2O$ (35 g/l) + $CuSO_4 \cdot 5H_2O$ (2 g/l) + $FeSO_4 \cdot 7H_2O$ (15 g/l) + H_3BO_3 (10 g/l) + ascorbic acid (10 g/l) and a constant voltage of -1.8 V for about 15 min. The pH value of the FeCoCu electrolyte was maintained constant at about 3.0.

The obtained nanowires were submitted to controlled thermal treatments in the temperature range from 300 to 800 °C under Ar atmosphere for 2 h. Particular attention has been paid to the sample annealed at 700 °C, which shows the highest coercivity.

The arrangement of the samples was checked in a FEI Helios NanoLab 600 FIB using the electron beam to obtain both the SEM images and the EDS microanalysis. Samples were thinned to lamellas by the ion beam to allow for HRTEM observation. The obtained lamellas contained several FeCoCu nanowires surrounded by the AAO template.

Nanowires inside the as-prepared membrane were in addition structurally characterized with a PANalytical X'pert Pro X-ray diffractometer (XRD) in Bragg-Brentano geometry using CuK_α lines. We also used a probe corrected TEM/STEM transmission electron microscope (FEI Titan G2 ChemiSTEM) working at 200 kV to perform elemental analyses, mappings, high angle annular dark field (HAADF) images, HRTEM images, and SAED patterns.

Finally, the magnetic properties of as-prepared and annealed nanowire arrays, particularly the hysteresis loops and their parameters, were measured in a vibrating sample

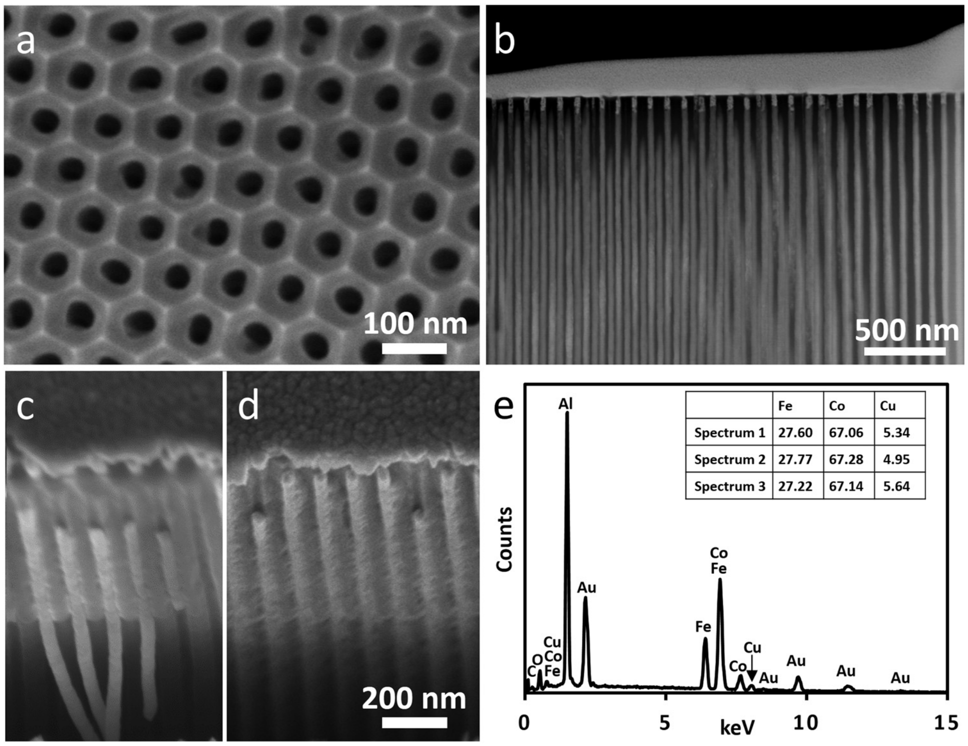

FIG. 1. (a) Top view of an empty alumina template. (b)–(d) Representative cross-section SEM images of FeCoCu nanowires within the AAO template. (e) EDS spectra and a table showing three semi-quantitative microanalysis results obtained in the top surface of the AAO-nanowires composite.

magnetometer (VSM) at room temperature, under a maximum field of ± 2 T applied parallel and perpendicular to the nanowires axis.

III. STRUCTURAL CHARACTERIZATION

Figure 1(a) shows the top view of an ordered AAO template before the electrodeposition of the wires. Figures 1(b)–1(d) show selected representative cross-section SEM images of the FeCoCu nanowires within the AAO membrane in the very same place where they were grown and show an almost perfect periodicity (Fig. 1(b)). From these figures, the average spacing between centers of the pores has been measured to be 93 nm, close to the expected 100–105 nm, a mean nanowires diameter of 40 nm, and a length of 8–10 μm. Images also show that nearly all the pores were filled. Figure 1(c) shows some nanowires bent out of the pores. Such bending was produced during the breaking of the AAO template to obtain cross-section SEM images and it demonstrates the malleability and metallic character of the nanowires.

Figure 1(e) displays a representative energy dispersive X-ray microanalysis spectrum (EDS) together with semi-quantitative EDS results obtained in three different regions at the surface of the AAO composite containing the FeCoCu nanowires. Because of the AAO template presence, Al is the most intense peak, while O is also detected. Gold peaks are due to the electrically conductive layer sputtered at the bottom of the template, and finally, Fe, Co, and Cu peaks correspond to the magnetic nanowires. The presence of the same elements in the nanowires has been also confirmed by STEM-XEDS mappings (see Fig. 3 below). From these semi-quantitative EDS results, we estimate an average composition of $Fe_{0.28}Co_{0.67}Cu_{0.05}$ for the nanowires.

The XRD spectra of the as-prepared FeCoCu nanowires embedded into the AAO template are shown in Fig. 2. Their reduced peaks intensity is a consequence of being embedded in the AAO template. Due to the lack of data about the crystal structure of the FeCoCu phases with such low Cu content, the diffraction peaks were indexed on the basis of the FeCo phases. The diffraction lines in the pattern matched quite well to the body centered cubic (*bcc*) structure of the FeCo, space group Im-3m (PDF2 Card No. 44-1433). This structure was previously reported for FeCo nanowires, where the Fe/Co ratio seems to be an important parameter to achieve wires with *bcc* or *fcc* phase.[30,31] The XRD pattern also shows a peak close to $2\theta = 38°$, which we assigned to Au (111) coming from the back side of the sample. It is also worth to mention that no additional XRD peaks were observed in the

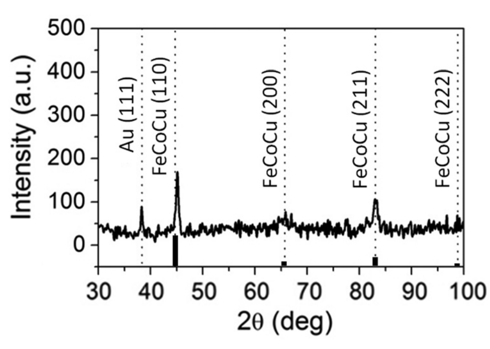

FIG. 2. XRD pattern of the as-prepared nanowires within the AAO template whose peaks correspond to body centered cubic (*bcc*) FeCoCu phase and to the back sputtered gold layer. Wide baseline bars represent the position and the intensity of a random orientation distribution of the *bcc* FeCo crystallites (extracted from the PDF2 Card No. 44-1433).

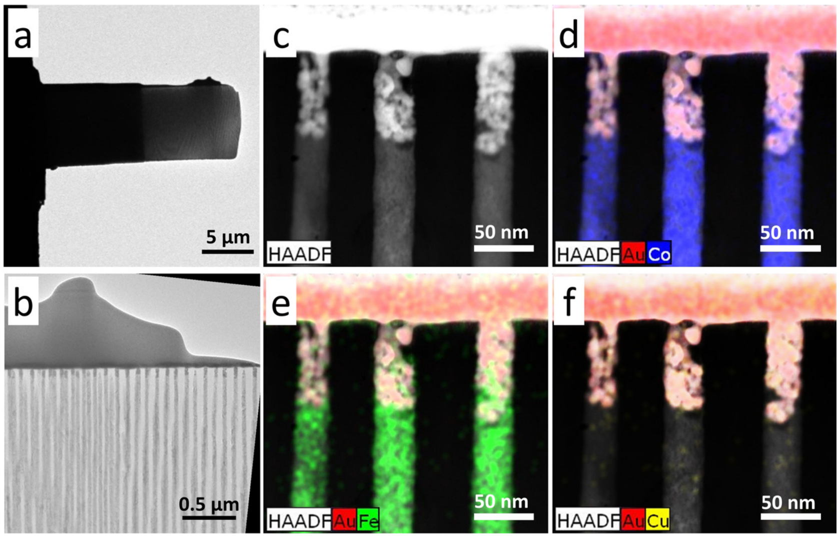

FIG. 3. (a) and (b) Lamella prepared from the as-prepared sample by FIB milling. (c) HAADF-STEM image showing Z-contrast. Brighter areas correspond to the top gold layer. (d)–(f) STEM-EDS elemental mappings showing the distribution of gold, cobalt, iron, and copper (note the reduced number of Cu points in (f)).

as-prepared sample corresponding to Fe, Co, or Cu oxides nor peaks corresponding to metallic Co (*fcc* or *hcp*).

From the peaks intensity in the XRD pattern, it is not possible to clearly identify a preferred orientation of the FeCoCu crystallites, probably due to the AAO presence. We can only point out the relatively higher intensity of the 211 peak as expected for a random orientation of the crystallites. That seems inconsistent with previous reports on FeCo nanowires grown in AAO, where a preferred orientation has been determined in the ⟨110⟩ direction.[32] As we will see below, electron diffraction data have confirmed the ⟨211⟩ direction as one of the two preferred orientation of the wires. Possible explanations for the discrepancy in the preferred orientation are differences in sample preparation, in pore diameter, or the actual electrodeposition conditions that lead to a different texture in the wires, as this has been previously proved by Baik *et al.*[33]

Figure 3(a) depicts a low magnification TEM image of a lamella obtained from the as-prepared sample, while Fig. 3(b) shows an image of the same lamella where the upper part of the parallel wires is already visible going down from the top Pt protective layer deposited in the FIB. Figure 3(c) corresponds to an HAADF-STEM image of some wires within the lamella showing mass-thickness contrast. In this picture, brighter areas correspond to higher atomic number or to thicker areas. Since lamellas have almost uniform thickness, we can assume that the differences in contrast are mainly due to differences in composition. This picture was acquired at the region showing the contact achieved between the FeCoCu wires and the conductive gold layer (at the top). These images also confirm the parallelism of the wires within the AAO template in vertical position. Figures 3(d)–3(f) correspond to STEM-EDS elemental mappings that confirm the presence of the top Au conductive layer, and that the wires composition includes cobalt, iron, and copper. It is interesting to emphasize that the Co and Fe distributions are nearly isotropic, discarding the deposition of grains of isolated elements and pointing to the formation of the alloy.

The Cu mapping is not as clear as those of Fe and Co because of its low content. Despite the long acquisition time, it is hard to obtain good STEM-EDS elemental mappings with such low Cu content.

In order to visualize the crystallites size and their distribution within the nanowires, bright field-dark field (BF-DF) studies were performed. Again, the nanowires were imaged in the lamellas as they were embedded in the AAO templates. Figures 4(a) and 4(b) show a pair of BF-DF images of the very same area of the lamella of as-prepared FeCoCu nanowires, while Figs. 4(c) and 4(d) correspond to the very same area on a sample after thermal treatment at 700 °C. In the BF images, the nanowires and the template are in perpendicular position respect to the electron beam, while the DF images were obtained as conical DF, using the {110} type reflections as working reflection, these reflections can be checked in Fig. 5. From the images of Fig. 4, we have estimated an average diameter of 40 nm for nanowires in the as-prepared sample (in agreement with the average value estimated from SEM images), and it reduces to about 37 nm for the annealed sample.

The comparative observation of the images of individual nanowires inside the template for as-prepared (Fig. 4(e)) and annealed (Fig. 4(f)) samples reveals the presence of an external region in the annealed nanowire with different contrast; this region can be checked in some places of Fig. 4(c) and is marked by the two arrows in Fig. 4(f). After careful analysis, we are inclining to suggest that in some places of the interface between the nanowire and the aluminum oxide, there is a gap that corresponds to the shrinkage of around 3 nm in the nanowires average diameter; connected with a thermal effect induced by the annealing.

In the DF images, we can observe large areas of the wires brighter than their average grey level. These brighter areas correspond to crystallites or grains with strong {110} diffracted beams, denoting their relative crystalline orientation with regards to the electron beam that fulfilled a particular diffraction condition. From a systematic study of these images, we can establish the polycrystalline nature of the nanowires, where some of the crystallites are as large as 200 nm. In the DF images, we observe that some crystallites fill completely the diameter of the nanopore, while in other cases two or more crystallites grow together to fill the pores diameter. An important feature to note is the presence of dark and bright stripes, or dark smaller areas within the

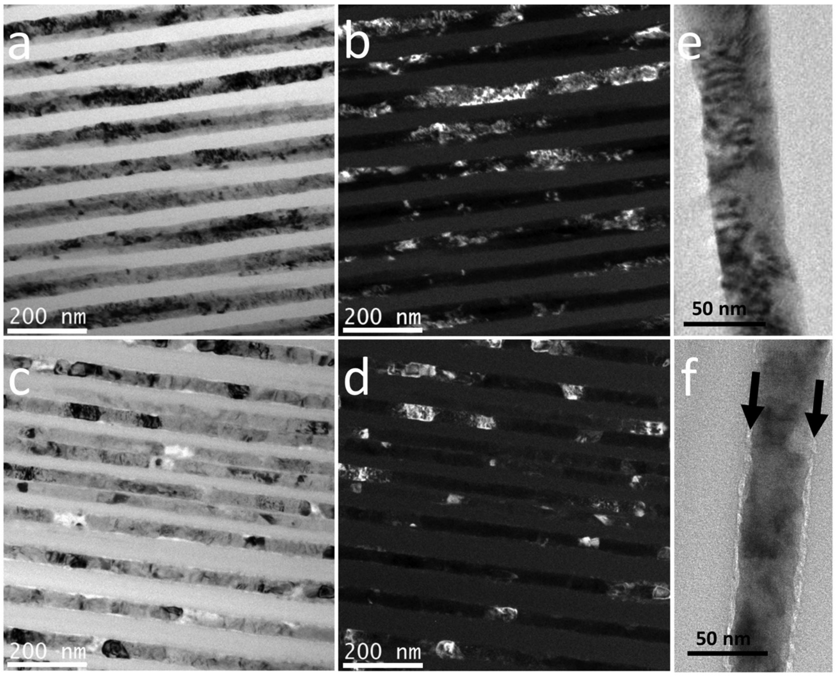

FIG. 4. Pair of bright field (BF) dark field (DF) images of the as-prepared (a) and (b), and 700 °C annealed samples (c) and (d) at the same location. The DF images were obtained as conical DF using the {110} type reflections as the working reflection, see text. Images of individual nanowires inside the template for as-prepared (e) and annealed (f) samples. In the annealed sample (f), a gap (marked by the two arrows) between the nanowire and the alumina is observed.

larger brighter areas which points to a lack of perfect crystalline grains and suggests the presence of extensive defects inside the grains. From the comparison between Figs. 4(b) and 4(d), we can conclude that, in general, the crystallite bounds are sharper in the annealed sample. This is ascribed to a recrystallization process induced by the annealing resulting in nanowires with smaller density of defects and better defined crystallites.

The crystalline structure of the FeCoCu nanowires has been also determined by SAED technique. Figures 5(a) and 5(c) show SAED patterns acquired from lamellas corresponding to as-prepared and annealed at 700 °C samples. Both patterns were obtained in areas limited by the SAED aperture displayed in the corresponding insets that included several wires within each lamella. The in-plane rotation of the patterns was compensated in such a way that the crystalline directions in the reciprocal and in the real spaces are parallel. The two ring patterns show diffraction rings not completely filled by the average in-plane rotation of the diffracted spots. In both patterns, only some angular sectors of each ring have strong intensity, which is an indication of the presence of a preferred orientation in the crystals that form the wires.

SAED provides additional information about the crystalline structure of the nanowires. The indexation of the SAED patterns (Figs. 5(a) and 5(c)), considering all the rings, complete or not, matched quite well with the Im-3m crystalline structure (*bcc* type) (Space Group No. 229), assuming a cubic cell parameter a = 2.85 Å.[8]

The type of SAED patterns displayed in Figs. 5(a) and 5(c), showing preferred orientation, is also known as textured patterns. In order to determine the crystallographic orientation of the nanowires axes, we plotted an arrow in the SAED pattern parallel to the wires. This arrow pointed to strong diffraction sectors of two rings corresponding to 112 and 222 indexes, with the maximum intensity in the 222 index where the arrow is well centered. As can be checked in Fig. 5(b), these two crystalline directions are not parallel in the Im-3m space group. The more simple explanation, for the occurrence of two strong sectors in rings corresponding to two not parallel directions, is to expect wires containing crystallites, or grains, with both preferential directions. Nevertheless, if we consider that there is only 19.47° between $\langle 112\rangle$ and $\langle 111\rangle$ directions in the [110] projection (Fig. 5(b)), an alternative explanation would consider the presence of both directions as a result of an average misorientation of the wires growing direction (i.e., due to the pores within the AAO template). These two alternatives are later discussed in more detail in view of HRTEM data.

Electron diffraction pattern of the sample annealed at 700 °C shows almost the same results as the as-prepared sample. The indexation of the rings, together with the analysis of the preferred orientation is shown in Fig. 5(c). The pattern also shows the $\langle 112\rangle$ and $\langle 111\rangle$ crystalline directions as the growing directions parallel to the nanowires. We should underline that the pattern is formed by more discrete spots, while the strong intensity sectors of each ring are less defined. We ascribe these changes to the effect of the annealing that probably yields more defined crystallites. Given the bright field-dark field results, it looks like the annealing increased the overall size of the grains and reduced the defects inside the grains. The electron diffraction pattern of the annealed sample also shows some additional spots that could not be assigned to the Im-3m crystalline structure of the FeCoCu. While the origin of these spots was not clearly identified in the sample annealed at 700 °C, it seems to be connected with a partial oxidation of the wires confirmed by XRD measurements (not shown in this paper).

The crystalline structure was further checked using the HRTEM for the as-prepared sample and after annealing at 700 °C. Improved HRTEM images, showing the lattice and the crystalline structure of the wires, were obtained focusing at the edges of the wires to avoid the overlapping of different crystallites. In this way, Fig. 6(a) shows a high quality

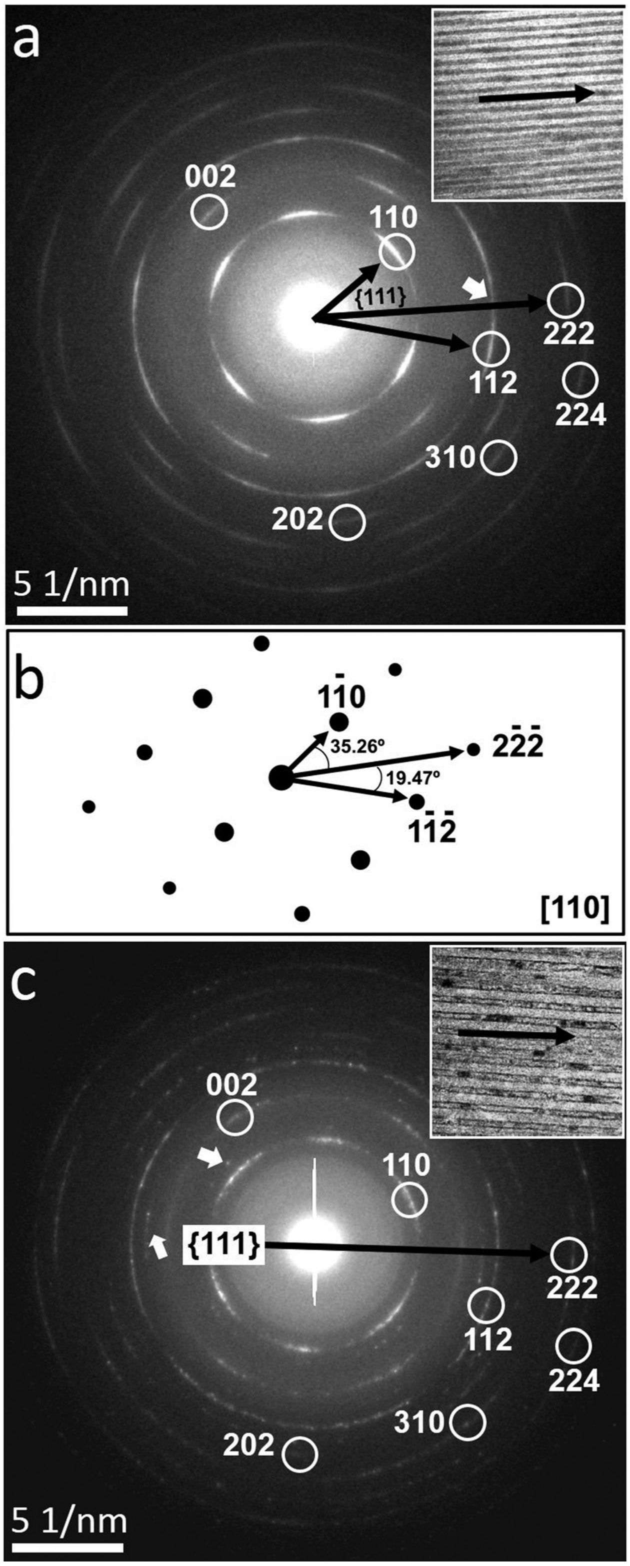

FIG. 5. (a) SAED pattern of the as deposited sample acquired in the area included by the aperture and shown in the inset. (b) Reciprocal lattice of the Im-3m space group in the [110] zone axis. (c) Same as (a) but for the sample annealed at 700 °C, some additional spots not indexed are pointed by the white arrows. In (a) and (c), the in-plane rotation of the patterns was compensated to show the crystalline growing direction of the wires parallel to the black arrow depicted in the insets.

HRTEM image at the edge of a selected nanowire from an as-prepared nanowire inside the AAO template. From the Fourier transform (FT) displayed in the inset, it was possible

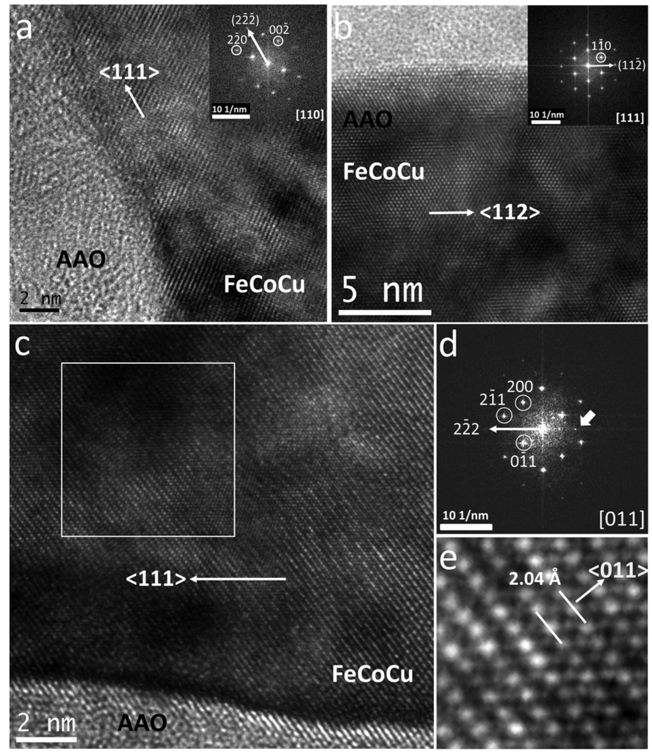

FIG. 6. (a) and (b) As-prepared sample, HRTEM images of the FeCoCu nanowires edge and part of the AAO template showing ⟨111⟩ and ⟨112⟩ crystalline directions parallel to the wire growing direction. The directions calculated from the respective Fourier transforms of the images are shown in the respective insets. (c) Sample annealed at 700 °C, HRTEM image showing one nanowire edge with the ⟨111⟩ direction as the growing direction. (d) Fourier transform of the area inside the box depicted in (c). (e) Close up showing the lattice image with a measured interplanar distance of 2.04 Å.

to determine the crystalline direction parallel to the growing direction of the nanowire. This FT pattern demonstrates the [011] zone axis of the Im-3m crystalline structure, and from that, we could calculate the indexes of the spots in the pattern. After that, it looks clear that the ⟨111⟩ crystalline direction is parallel to the average direction of the nanowire. Figure 6(b) shows a very different situation corresponding to a different area at the edge of an as-prepared nanowire within the alumina. The indexed FT pattern in the inset demonstrates that, in this case, the average main axis of the nanowire is parallel to the ⟨112⟩ crystalline direction. The analysis of these two particular cases for individual crystals in the nanowires local edges confirms the existence of two growing directions, ⟨111⟩ and ⟨112⟩, both in complete agreement with the data obtained by SAED and also partially with XRD data.

In Fig. 6(c), we show a HRTEM image at the edge of a FeCoCu nanowire corresponding to the sample annealed at 700 °C, where the ⟨111⟩ crystalline direction is parallel to the main axis of the wire. In this image, we observe two interesting details: (i) the edge of the wire is neither perfectly flat nor fully parallel to the ⟨111⟩ crystalline direction, and (ii) the image shows faint Moiré patterns probably due to some overlapping crystallites. The FT pattern displayed in Fig. 6(d) reveals the presence of additional spots, which cannot be justified based on a perfect Im-3m structure. One of the spots, marked by a white arrow, is clearly not in the same reciprocal net as the main spots. The origin of such unidentified spots can be ascribed to the presence of tiny crystallized AAO remains, to small defects in the crystallites, or even to some tiny crystalline domains with different structure. We should note that no clear evidence of the presence of crystalline phases other than the *bcc* type was found at least in the as-prepared samples. Figure 6(e) shows a closer view of the lattice image of the as-prepared FeCoCu nanowires that allowed us the evaluation of the interplanar distances of the crystal structure in the HRTEM images. An interplanar distance of 2.04 Å has been measured in the $\langle 011 \rangle$ crystalline direction which, within the experimental TEM error, is close to the data reported previously for the $Fe_{1-x}Co_x$ with x in the range between 0.62 and 0.82.[34] These results further confirm the Im-3m crystalline structure for the FeCoCu nanowires.

IV. MAGNETIC MEASUREMENTS

The hysteresis loops under applied magnetic field parallel to the nanowires axis have been measured at room-temperature for as-prepared samples and after annealing in the temperature range from 300 to 800 °C (Fig. 7(a)). For a better description of the influence of thermal treatments, the evolution of coercivity and squareness (ratio of remanence to saturation magnetization, M_r/M_s) are shown in Fig. 7(b). As observed, the squareness takes a value of 0.71 in the as-prepared state, and it increases gradually by increasing the annealing temperature and reaches a maximum of 0.91 for the sample annealed at 700 °C and then decreases to 0.74 by further increasing the annealing temperature to 800 °C. Squareness takes very small values (less than 0.1) in the case of hysteresis loops under applied field perpendicular to the nanowires. The inset in Fig. 7(a) shows an example of hysteresis loop measured with the field applied perpendicular to the as-prepared nanowires. Consequently, we can deduce that in all the cases, the magnetization easy axis lies along the nanowires axis (i.e., perpendicular to the membrane's plane).

Similar evolution was observed (see Fig. 7(b)) for the coercivity. Again, the coercivity increases with annealing temperature and reaches a maximum after annealing at 700 °C, then it decreases by increasing further the annealing temperature. It is also worth to mention that apart from the increase in coercivity and remanence, a small decrease in the value of saturation magnetization at room temperature was observed for the sample after annealing at increasing temperatures (i.e., from 2.0 T in as-prepared state, a maximum decrease down to 1.7 T is observed after annealing at 700 °C). This magnetic hardening with thermal treatment, previously observed in the case of arrays of FeCoCu nanowires 18 nm in diameter, was there interpreted as arisen from the transition of vortex to transverse domain-wall magnetization reversal modes essentially connected with the mentioned reduction of saturation magnetization

The observed modifications of the magnetic behavior with annealing are expected to be connected with the parallel modifications of the structure. The present structural study has been performed in nanowires inside the template, and we have confirmed that FeCoCu nanowires present *bcc* polycrystalline structure (matching the Im-3m structure) with $\langle 111 \rangle$ and $\langle 112 \rangle$ as preferred directions of crystallites parallel to the wires axes. After thermal treatments up to 700 °C, the optimal temperature for achieving magnetic hardening, we observe that essentially the structure remains the same. However, the following minor differences are observed: (i) the crystals increased sizes, their bounds are sharper, and there is a significant reduction of crystalline defects (deduced qualitatively from BF-DF images, see Figs. 4(a) to 4(d)); (ii) traces of tiny crystalline domains with different structure are found in the annealed sample, which cannot be justified based on a perfect Im-3m structure, see Fig. 6(d), and (iii) shrinkage effect in the nanowires diameter (from HRTEM of individual nanowires inside the alumina, see Figure 4(f)). The increased and sharper shape of crystallites in point (i) suggests an increase in the effective magnetocrystalline anisotropy and of pinning for domain walls.[35] That would contribute to the magnetic hardening as proposed in the micromagnetic simulations, where a transition from vortex to transverse domain-wall magnetization reversal mode occurs.[28] The traces of tiny unidentified crystals mentioned in point (ii) could be an additional origin for the pinning of domain walls and effective crystalline anisotropy as well. Then, the reduction of diameter mentioned in point (iii) should result in enhanced coercivity according to micromagnetic modeling.[33,36] Note in addition that the heating of the nanowires is performed under geometrical confinement, which can lead on one hand to relief of stresses accumulated during electroplating but also can give rise to a net magnetostrictive anisotropic effect owing to a mismatch between the thermal expansion coefficients (α) of FeCo alloys ($\alpha = 14 \times 10^{-6}\,K^{-1}$) and alumina ($\alpha = 6 \times 10^{-6}\,K^{-1}$),

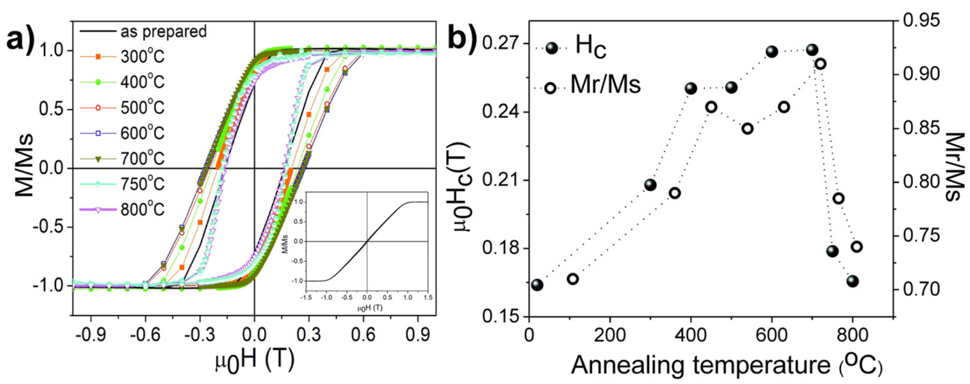

FIG. 7. Hysteresis loops for arrays of FeCoCu nanowire in as-prepared state and after annealing at different temperatures with the field applied parallel and perpendicular (inset) to the nanowire axis (a). Evolution of coercivity, *Hc*, and squareness (*Mr*/*Ms*) as function of the annealing temperature (b).

which will produce an expansion of the alloy along the nanowire axis.[35,37,38]

The final decrease of coercivity after annealing above 700 °C has been ascribed to the increase of the internal stress that introduces a distortion of the pores parallelism, which seemingly reduces the axial anisotropy resulting in a reduction of coercivity and squareness.[35] The strength of such stresses is relevant in arrays of nanowires of different diameter and interwire distance to determine the annealing temperature to achieve the maximum magnetic hardening. In addition, we should finally mention that the presence of Co oxides has been observed after annealing at the highest temperatures, which appearance is very critical and might correlate also with first stages leading to the deterioration of the magnetic properties. This matter is anyway beyond the objectives of the present study.

V. CONCLUSIONS

FeCoCu nanowire arrays have been fabricated by DC electrodeposition filling the self-assembled pores of AAO templates. Samples were thermally treated in the range of temperature between 300 and 800 °C, and then characterized at room temperature. Most attention has been paid to as-prepared sample and after annealing at 700 °C for which we observe the maximum effect on the magnetic properties.

The nanowires structure has been determined while embedded in the templates. Particularly, we imaged the wires inside the AAO template using transmission electron microscopy through FIB sample preparation. They show *bcc* crystalline structure that matches the Im-3m space group, while $Fe_{0.28}Co_{0.67}Cu_{0.05}$ composition was determined using EDS microanalysis.

Almost all of the pores were filled and the obtained wires, 40 nm in diameter, were separated by a distance of 93 nm between centers. SAED images demonstrated textured patterns both in as-prepared and in annealed samples, with $\langle 111 \rangle$ and $\langle 112 \rangle$ preferred growth directions also confirmed by HRTEM images and their FT analyses.

After heating treatment at 700 °C, the polycrystalline nanowires recrystallized to result in better crystallized grains with smaller amount of defects. In addition, tiny traces of unidentified crystals were found with different crystalline structure, while a shrinkage effect in the nanowires diameter was also observed.

These structure changes contribute to the observed modified magnetic behavior which maximum hardening was observed when annealing at 700 °C.

ACKNOWLEDGMENTS

This work was supported by the European Community's 7th Framework Program under Project REFREEPERMAG, Grant No. 280670, and by the Spanish Ministerio de Economia y Competitividad under Project MAT2010-0278-C05-01. T. Warnatz acknowledges DAAD grant supporting his visit to laboratories in Madrid.

[1] C. R. Martin, Science **266**, 1961 (1994).
[2] A. Huczko, Appl. Phys. A **70**, 365 (2000).
[3] N. Gao, H. Wang, and E.-H. Yang, Nanotechnology **21**, 105107 (2010).
[4] E. Ferain and R. Legras, Nucl. Instrum. Methods Phys. Res., Sect. B **267**, 1028 (2009).
[5] D. Atkinson, D. A. Allwood, G. Xiong, M. D. Cooke, C. C. Faulkner, and R. P. Cowburn, Nature Mater. **2**, 85 (2003).
[6] J. M. García, A. Asenjo, J. Velázquez, D. García, M. Vázquez, P. Aranda, and E. Ruiz-Hitzky, J. Appl. Phys. **85**, 5480 (1999).
[7] H. L. Su, G. B. Ji, S. L. Tang, Z. Li, B. X. Gu, and Y. W. Du, Nanotechnology **16**, 429 (2005).
[8] G. H. Yue, L. S. Wang, X. Wang, Y. Z. Chen, and D. L. Peng, J. Appl. Phys. **105**, 074312 (2009).
[9] L. G. Vivas, J. Escrig, D. G. Trabada, G. A. Badini-Confalonieri, and M. Vazquez, Appl. Phys. Lett. **100**, 252405 (2012).
[10] V. Vega, T. Böhnert, S. Martens, M. Waleczek, J. M. Montero-Moreno, D. Görlitz, V. M. Prida, and K. Nielsch, Nanotechnology **23**, 465709 (2012).
[11] L. G. Vivas, Y. P. Ivanov, D. G. Trabada, M. P. Proenca, O. Chubykalo-Fesenko, and M. Vázquez, Nanotechnology **24**, 105703 (2013).
[12] Y. Xia, P. Yang, Y. Sun, Y. Wu, B. Mayers, B. Gates, Y. Yin, F. Kim, and H. Yan, Adv. Mater. **15**, 353 (2003).
[13] C. Schönenberger, B. M. I. Van Der Zande, L. G. J. Fokkink, M. Henny, C. Schmid, M. Krüger, A. Bachtold, R. Huber, H. Birk, and U. Staufer, J. Phys. Chem. B **101**, 5497 (1997).
[14] G. E. Thompson, Thin Solid Films **297**, 192 (1997).
[15] O. Jessensky, F. Müller, and U. Gösele, Appl. Phys. Lett. **72**, 1173 (1998).
[16] S. J. Limmer, S. Seraji, Y. Wu, T. P. Chou, C. Nguyen, and G. Z. Cao, Adv. Funct. Mater. **12**, 59 (2002).
[17] Y. Li, D. Xu, Q. Zhang, D. Chen, F. Huang, Y. Xu, G. Guo, and Z. Gu, Chem. Mater. **11**, 3433 (1999).
[18] X. Y. Zhang, L. D. Zhang, W. Chen, G. W. Meng, M. J. Zheng, L. X. Zhao, and F. Phillipp, Chem. Mater. **13**, 2511 (2001).
[19] T. M. Whitney, J. S. Jiang, P. C. Searson, and C. L. Chien, Science **261**, 1316 (1993).
[20] R. Inguanta, S. Piazza, and C. Sunseri, Appl. Surf. Sci. **255**, 8816 (2009).
[21] M. P. Proenca, C. T. Sousa, J. Ventura, M. Vazquez, and J. P. Araujo, Electrochim. Acta **72**, 215 (2012).
[22] V. Haehnel, S. Fähler, P. Schaaf, M. Miglierini, C. Mickel, L. Schultz, and H. Schlörb, Acta Mater. **58**, 2330 (2010).
[23] K. S. Napolskii, I. V. Roslyakov, A. A. Eliseev, D. I. Petukhov, A. V. Lukashin, S.-F. Chen, C.-P. Liu, and G. A. Tsirlina, Electrochim. Acta **56**, 2378 (2011).
[24] C. Bran, Y. P. Ivanov, D. G. Trabada, J. Tomkowicz, R. P. del Real, O. Chubykalo-Fesenko, and M. Vazquez, IEEE Trans. Magn. **49**, 4491 (2013).
[25] Y. Peng, T. Cullis, G. Möbus, X. Xu, and B. Inkson, Nanotechnology **18**, 485704 (2007).
[26] H. Pan, B. Liu, J. Yi, C. Poh, S. Lim, J. Ding, Y. Feng, C. H. A. Huan, and J. Lin, J. Phys. Chem. B **109**, 3094 (2005).
[27] R. L. Wang, S. L. Tang, Y. G. Shi, X. L. Fei, B. Nie, and Y. W. Du, J. Appl. Phys. **103**, 07D507 (2008).
[28] C. Bran, Y. P. Ivanov, J. García, R. P. del Real, V. M. Prida, O. Chubykalo-Fesenko, and M. Vazquez, J. Appl. Phys. **114**, 043908 (2013).
[29] B. Rodríguez-González, F. Vereda, J. de Vicente, and R. Hidalgo-Álvarez, J. Phys. Chem. C **117**, 5397 (2013).
[30] P. S. Fodor, G. M. Tsoi, and L. E. Wenger, J. Appl. Phys. **91**, 8186 (2002).
[31] H. Moumeni, S. Alleg, and J. M. Greneche, J. Alloys Compd. **386**, 12 (2005).
[32] S. Tang, W. Chen, M. Lu, S. Yang, F. Zhang, and Y. Du, Chem. Phys. Lett. **384**, 1 (2004).
[33] J. M. Baik, M. Schierhorn, and M. Moskovits, J. Phys. Chem. C **112**, 2252 (2008).
[34] Q. Zhan, Z. Chen, D. Xue, F. Li, H. Kunkel, X. Zhou, R. Roshko, and G. Williams, Phys. Rev. B **66**, 134436 (2002).
[35] D.-H. Qin, Y. Peng, L. Cao, and H.-L. Li, Chem. Phys. Lett. **374**, 661 (2003).
[36] Y. P. Ivanov, M. Vázquez, and O. Chubykalo-Fesenko, J. Phys. D: Appl. Phys. **46**, 485001 (2013).
[37] K. R. Pirota, E. L. Silva, D. Zanchet, D. Navas, M. Vázquez, M. Hernández-Vélez, and M. Knobel, Phys. Rev. B **76**, 233410 (2007).
[38] L. Cao, X. Qiu, J. Ding, H. Li, and L. Chen, J. Mater. Sci. **41**, 2211 (2006).